

A DGS pattern including DMS behavior for compact unit-cell designs

Jorge Aguilar-Torrentera^{a)}, Moisés Hinojosa-Rivera,
and Javier Morales-Castillo

*Universidad Autónoma de Nuevo León, Electrical Eng. Faculty,
Pedro de Alba S/N, Monterrey 66450, México*

a) jorge.aguilart@uanl.mx

Abstract: In this paper, a new (defected ground structure) DGS unit-cell is introduced and its performance is analyzed. The dumbbell-shaped DGS cell is modified by etching off slots in the ground plane to include (defected microstrip structure) DMS behavior without etching any defect in the microstrip line. The degree of freedom of cell design allows setting the bandgap center frequency while enabling a degree of miniaturization. A circuit-model is proposed to provide accurate cell responses. Simulations of the unit-cell with DGS and DMS behavior show moderate electromagnetic (EM) noise from the ground plane. Advantages are illustrated in a fabricated cell occupying approximately 40% less area.

Keywords: electromagnetic bandgap, defected ground structures (DGS), defected microstrip structures (DMS) and circuit-model equivalence

Classification: Microwave and millimeter-wave devices, circuits, and modules

References

- [1] A. Kumar and K. Machavaram: “Microstrip filter with defected ground structure: A close perspective,” *Int. J. Microw. Wirel. Technol.* **5** (2013) 589 (DOI: [10.1017/S1759078713000639](https://doi.org/10.1017/S1759078713000639)).
- [2] M. K. Khandelwal, *et al.*: “Defected ground structure: Fundamentals, analysis and applications in modern wireless trends,” *Int. J. Ant. Prop.* **2017** (2017) 2018527 (DOI: [10.1155/2017/2018527](https://doi.org/10.1155/2017/2018527)).
- [3] J.-S. Lim, *et al.*: “A vertically periodic defected ground structure and its application in reducing the size of microwave circuits,” *IEEE Microw. Wireless Compon. Lett.* **12** (2002) 479 (DOI: [10.1109/LMWC.2002.805941](https://doi.org/10.1109/LMWC.2002.805941)).
- [4] M. K. Mandal and S. Sanyal: “A novel defected ground structure for planar circuits,” *IEEE Microw. Wireless Compon. Lett.* **16** (2006) 93 (DOI: [10.1109/LMWC.2005.863192](https://doi.org/10.1109/LMWC.2005.863192)).
- [5] A. Abdel-Rahman, *et al.*: “Control of bandstop response of Hi-Lo microstrip low-pass filter using slot in ground plane,” *IEEE Trans. Microw. Theory Techn.* **52** (2004) 1008 (DOI: [10.1109/TMTT.2004.823587](https://doi.org/10.1109/TMTT.2004.823587)).
- [6] C.-S. Kim, *et al.*: “Equivalent circuit modelling of spiral defected ground structure for microstrip line,” *Electron. Lett.* **38** (2002) 1109 (DOI: [10.1049/el:20020742](https://doi.org/10.1049/el:20020742)).
- [7] M. Kazerooni, *et al.*: “Analysis, modeling, and design of cascaded defected

- microstrip structure for planar circuits,” *Int. J. RF Microw. Comput.-Aided Eng.* **20** (2010) 171 (DOI: [10.1002/mmce.20419](https://doi.org/10.1002/mmce.20419)).
- [8] J. Tirado-Mendez, *et al.*: “Improving frequency response of microstrip filters, using defected ground and defected microstrip structures,” *Prog. Electromagn. Res. C* **13** (2010) 77 (DOI: [10.2528/PIERC10011505](https://doi.org/10.2528/PIERC10011505)).
- [9] A. Boutejdar, *et al.*: “High-performance wide stop band low-pass filter using a vertically coupled DGS-DMS-resonators and interdigital capacitor,” *Microw. Opt. Technol. Lett.* **56** (2014) 87 (DOI: [10.1002/mop.28031](https://doi.org/10.1002/mop.28031)).
- [10] H.-M. Kim and B. Lee: “Bandgap and slow/fast-wave characteristics of defected ground structures (DGSs) including left-handed features,” *IEEE Trans. Microw. Theory Techn.* **54** (2006) 3113 (DOI: [10.1109/TMTT.2006.877060](https://doi.org/10.1109/TMTT.2006.877060)).

1 Introduction

Owing to its high performance, low cost and easy fabrication, the DGS has been adopted in several fields such as planar filters, amplifiers, antennas; etc. There have been proposed modifications of the conventional DGS pattern [1, 2] as a method to attain a degree of miniaturization of low-pass filters [3] and amplifiers [4]. Different slot heads occupying small area have been proposed to attain enhanced sharpness factors (rectangle slot [5]), deep rejection bands (H-headed [4]) and low resonance frequency (spiral defect [6]). These compact structures earn current flow in the ground plane of the microstrip line to achieve specific equivalent inductance and capacitance that shape aperiodic [5, 4] or periodic [6] responses. The DMS is another type of bandgap structure [7]. Its low field leakage and ease of integration make it an interesting option to complement to DGS [8, 9].

In this paper, we introduce the DMS behavior as a method to decrease the current flow around the apertures of the dumbbell shaped DGS at frequencies at which the associated capacitance of the microstrip line is dominant [1]. The proposed pattern increases the range of controllable inductance and capacitance otherwise limited in designs where the conventional DGS cell is used. The DMS behavior produces low insertion losses and bandstop responses with quality factors similar to those achieved by long T-shaped DMS unit-cells. Another advantage is its moderate radiated energy level below the ground plane at high frequencies, which is an important advantage for filter and antenna applications.

2 Proposed DGS pattern

The T-cell DMS pattern was originally introduced in [8] and is illustrated in Fig. 1a. It consists of a slot of length (L_s) and width (W_s) introduced over the microstrip line as well as a small discontinuity that separates stubs by a distance W_e . Our proposal is based on a modification of the dumbbell-shaped DGS in Fig. 1b. The DMS behavior is incorporated by etching slots bent in right-angle, as shown in Fig. 1c. “L” shaped slots are placed at both edges of the lattices of the DGS just beneath the microstrip line.

In the microstrip line with conventional DGS in Fig. 1b, the return current is fully distributed on the ground plane forming current paths around the periphery of

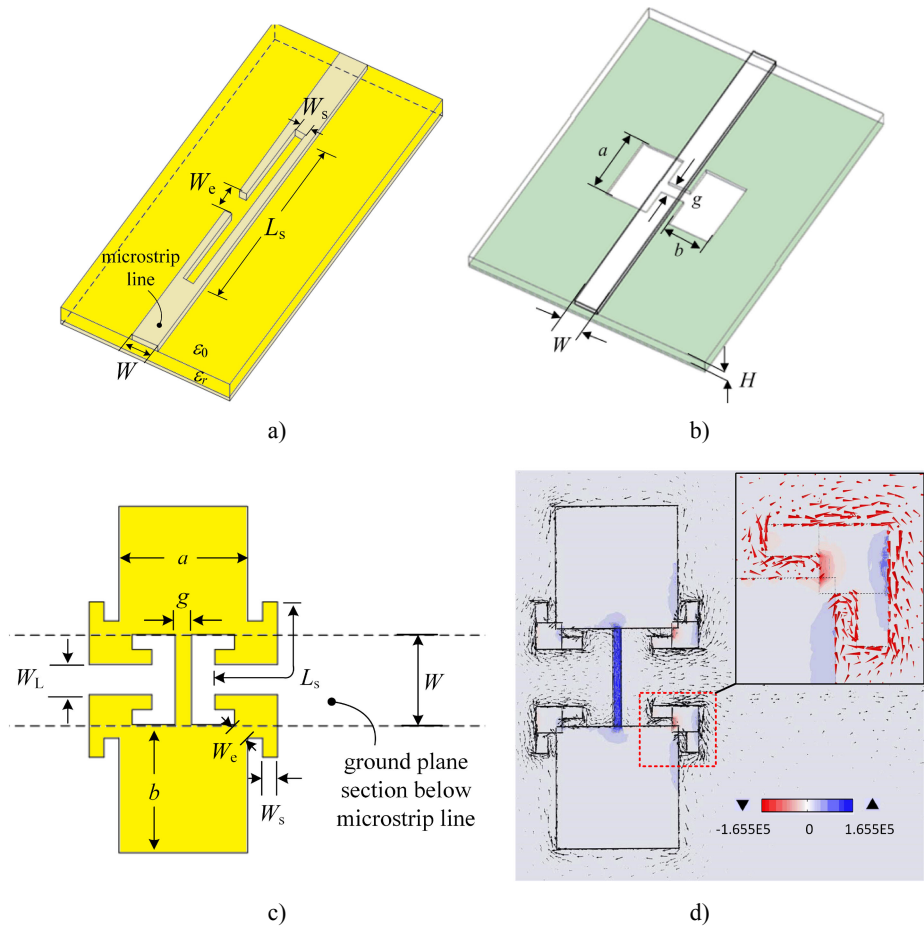


Fig. 1. a) Three-dimensional view of the dumbbell-shaped DGS, b) Three-dimensional view of the T-shaped DMS, c) Backside view of the proposed unit-cell, and d) EM simulation results of the surface current density and the outflow power at 7.7 GHz.

the square lattices (of dimension $a \times b$) to create an inductive effect [2]. In the new cell pattern, EM fields below the microstrip line perturb the return current to increase further the current path length. Fig. 1d shows EM simulation results of the L-slot DGS unit-cell at resonant frequency using COMSOL[®] V5.2. The inset depicts the surface current vector following a trajectory similar to that observed for the T-shaped DMS cell [7, 8]. Also in Fig. 1d are the filled contours of the normal component of the density power vector. A substantial field leakage underneath the microstrip line stems from the electric field trapped in the gap. For the DGS cell, the associated capacitive effect is associated to this discontinuity [2].

It is seen from Fig. 1d that the current around the slot retraces a path around the slots giving rise to an increased surface current density crossing the slots. Once this perturbation is over, the current flowing beneath the microstrip line is augmented, which results in an increased inductance of the line depending on the distance between slots chosen (W_L , see Fig. 1c). At frequencies at which the microstrip line presents a dominant capacitive effect, the DMS effect regulates the current flowing around the periphery of the square lattices to reduce magnetic flux, which alleviates the harmful energy radiation through the apertures.

EM simulations of the microstrip with L-slot DGS cell were carried out using substrate RT/Duroid 5880 with 31-mil-thick and dielectric constant ϵ_r of 3.66. The

line width (W) is chosen to be equal to 2.44 mm for a characteristic impedance of 50Ω for a typical microstrip line. Fig. 2 displays S -parameters of the new cell design and allows contrasting with responses of the dumbbell-shaped DGS. For L-slot DGS cells, the slots dimensions are $W_s = 0.3$ mm, $W_e = 0.3$ mm. The slot length was varied according with the distance between slots $W_L:L_s = 1.7$ mm, $W_L = 1.7$ mm; $L_s = 2.12$ mm, $W_L = 1.31$ mm and $L_s = 3.06$ mm, $W_L = 0.34$ mm.

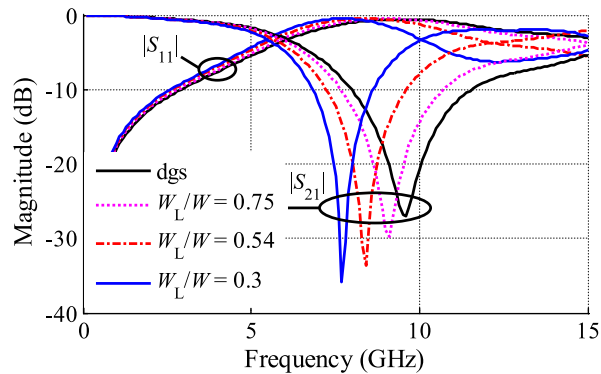


Fig. 2. Simulated S -parameters of unit-cells. The lattice dimension for all cells are $a = 3.0$ mm, $b = 3.0$ mm and gap distance, $g = 0.2$ mm.

Fig. 2 shows that attenuation poles and steep rejection characteristics vary with W_L . Reactive effects have some influence on the cut-off frequencies. In contrast, attenuation poles exhibit larger shifting at lower frequencies. For the case with ratio $W_L/W = 0.3$, the sharpness factor [2] is equal to 1.43, which is similar to that of the rectangle-slot cell in [5]. In addition, the attenuation band results to be better than -30 dB, which compares favorably to the H-headed DGS cell [4].

Reported area savings (regarding to the DGS pattern) are about 61% and 87% for H-headed and rectangle-slot cells; respectively. It is worth mentioning that comparative studies points out the slot-headed (arrow-shape) as the best option from the set of unit-cell patterns proposed in [5] given that implementations based on the rectangle-slot makes difficult handling radiation losses by shielding.

3 Circuit-model equivalence

The circuit-model in Fig. 3a provides a method to characterize performance of L-slot DGS cells. The equivalence comprises a lossless stub of characteristic impedance (Z_s) terminated with an ohmic resistance (R) and connected in parallel with an inductor and capacitor. The new cell is analyzed like the Butterworth one-pole low pass filter in Fig. 3b using the same procedure for the conventional DGS cell [1, 2]. The reactance of the parallel LC circuit (X_{LC}) should describe simultaneously the characteristics of a low-pass and bandstop filters with a single attenuation pole.

A stub is included to enhance the circuit-model equivalences. The input impedance of the stub should exhibit a zero reactive component at resonance so that the resistive load incorporated by the stub is equal to the associated radiation resistance. This requirement is met by the quarter-wave transformer hence the appropriate phase length of the stub (θ) is set to be equal to $\pi/2$ at the resonant frequency (ω_0). In modeling results, losses are associated only to radiation given

that loss-free dielectric material and Perfect Electric Conductor in metals were used in simulations.

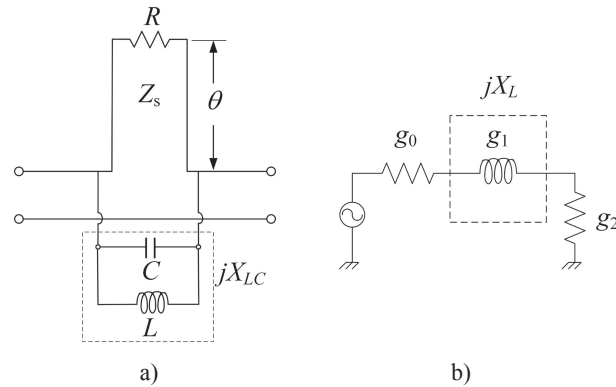


Fig. 3. a) Equivalent circuit of the DGS-DMS unit-cell. b) Butterworth-type one-pole lowpass filter (normalized prototype [1]).

A microstrip line with L-slot DGS cell was designed using the parameters itemized in Table I. The ratio W_L/W is equal to 0.73. EM simulation results of the cell design are displayed in Fig. 4. Using the extraction procedure in [1, 2], the equivalent capacitance is given by (1).

$$C = \frac{\omega_c}{2Z_0(\omega_0^2 - \omega_c^2)} \quad (1)$$

with $\omega_0 = 1/\sqrt{LC}$, Z_0 is the characteristic impedance and ω_c is the 3 dB cut-off frequency. From Fig. 4, the cut-off frequency and resonant frequency of the cell design are 3.26 GHz and 5.95 GHz, respectively, and those are substituted into (1) yielding a capacitance equal to 0.21 pF. All of the above results in an equivalent inductance of 3.41 nH. Using L and C values, the extraction of R and Z_s is achieved by optimization. The aim is at minimizing differences between the magnitudes of S-parameters at high frequencies. Table I lists the extracted circuit values.

Table I. Cell design parameters and extracted equivalent circuit-model elements.

Cell dimensions	Value (mm)	Extracted elements	Value
$a \times b$	5.0×5.0	Electrical length, θ (rad)	$\pi/2$ at ω_0
g	0.13	Impedance of stub, Z_s (Ω)	918.0
L_s	3.9	Termination resistance, R (Ω)	479.1
W_s	0.3	Equivalent capacitance, C (pF)	0.21
W_e	0.3	Equivalent inductance, L (nH)	3.41

The admittance of the LC -stub model in Fig. 3a is denoted by (2).

$$Y_s = j\omega_0 C \left(\frac{\omega}{\omega_0} - \frac{\omega_0}{\omega} \right) + \frac{1}{Z_s} \coth(\alpha + j\theta), \quad (2)$$

with $\alpha = \tanh^{-1}(R/Z_s)$ and $\theta = (\pi\omega)/(2\omega_0)$. From (2), the impedance of the cell at resonance is equal to the ratio $(Z_s)^2/R$ yielding an equivalence of 1758.9 Ω . Such radiation resistance results to be higher than that for a conventional DGS cell, which is in the range of 600–1500 Ω . [10]

At frequencies different from resonant, the stub shows a complex input impedance, which is explained by the standing wave on the matching section of the quarter-wave transformer. For a SWR = 1.91, the stub introduces a low capacitive susceptance at the cut-off frequency (3.26 GHz, $\theta \approx \pi/4$) and the 3-dB point is set fundamentally by the resonator. Fig. 4a allows contrasting the application of circuit-model methods. The LC-stub equivalence exhibits lower differences with EM simulations than for the Butterworth one-pole response.

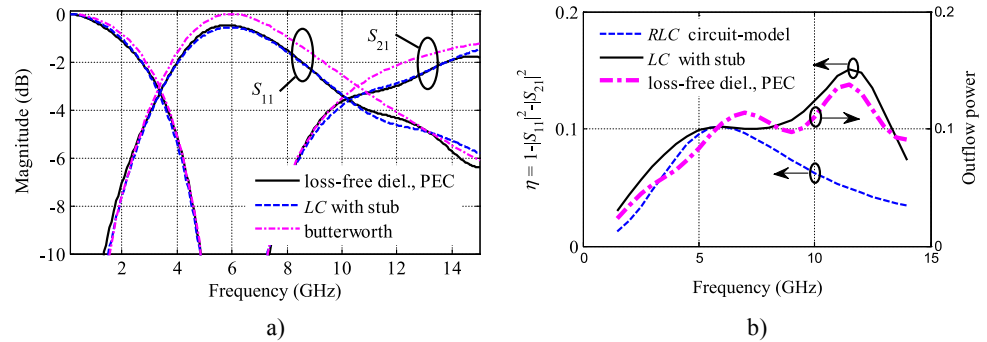


Fig. 4. a) S -parameters of the DGS-DMS unit-cell and responses of circuit-model equivalences, b) Radiation rate factor and EM radiation losses, RLC : $R = 1758.9 \Omega$, $L = 3.48 \text{ nH}$ and $C = 0.2058 \text{ pF}$ LC -stub: $L = 3.48 \text{ nH}$, $C = 0.2058 \text{ pF}$, $Z_s = 918.0 \Omega$ and $R = 479.1 \Omega$

The LC -stub method can provide accurate circuit-models for cells presenting moderate radiation losses. To analyze this capability, the radiation rate factor (η) was computed using circuit-model equivalences [2]. The radiation rate factor is displayed in Fig. 4b along with the radiation loss computed by EM field simulation. At the resonant frequency (5.95 GHz), the RLC and the LC -stub equivalences predict practically the same radiation loss than that based on EM outflow power computations (0.102). Nonetheless, at higher frequencies, the LC -stub method predicts variations of the radiation rate factor similar to those computed by outflow field assuming absorption boundary conditions. In contrast, the RLC method [10] appears to be inappropriate for predicting the radiation rate at higher frequencies.

4 L-slot DGS cell performance

We make use of the enhanced slow-wave factor of the new pattern to implement a compact unit-cell. To give assessment, the dumbbell shaped DGS and the proposed shaped DGS were designed to resonate at 7.7 GHz. Both designs have the same gap distance, $g = 0.2 \text{ mm}$. For the conventional DGS cell, the dimensions of the lattices are $4.1 \text{ mm} \times 4.1 \text{ mm}$ and for the new cell the dimensions are $3.0 \text{ mm} \times 3.0 \text{ mm}$. This represents a reduction factor of about 40%. Fig. 5 shows photographs of the fabricated unit-cell. For the slots bent in right angle: $W_s = 0.2 \text{ mm}$, $W_e = 0.2 \text{ mm}$, $L_s = 1.2 \text{ mm}$ and $W_L/W = 0.35$. Fig. 6a displays measurements of the fabricated prototype showing good agreement with EM simulation results.

Fig. 6b allows comparing frequency responses of the proposal with those of conventional cells resonating at 7.7 GHz. The DMS has $L_s = 11.5 \text{ mm}$ and $W_e = 0.2 \text{ mm}$. The dumbbell-shaped DGS has lattices of $3.5 \text{ mm} \times 3.5 \text{ mm}$ and a gap

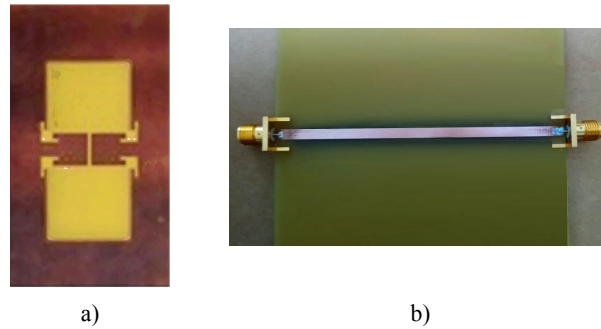


Fig. 5. Fabricated prototype (a) Bottom view (zoomed in for DGS-DMS detail), (b) Top view.

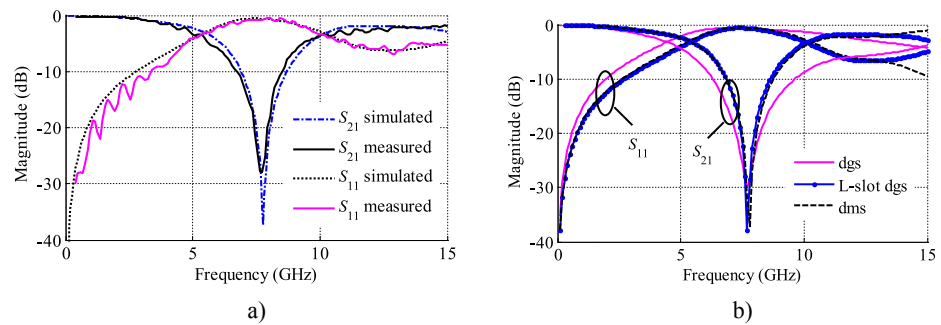


Fig. 6. a) Measured responses of L-slot shaped DGS and b) Comparison of the L-slot DGS with conventional structures resonating at 7.7 GHz.

distance of 4 mils (= 0.1016 mm), which is the narrower slot limit posed by inexpensive PCB fabrication process, was chosen to realize a cut-off frequency of 4.72 GHz. Good matching between the lengthwise compact cell and the T-shaped DMS cell both showing a cut-off frequency equal to 5.34 GHz is apparent. In order for the dumbbell-shaped DGS to achieve the sharpness factors of the responses in Fig. 6b, the gap distance should be equal to 55.0 μm (about a half of the minimum distance allowed by fabrication) while designing with the same size of apertures used for the L-slot DGS cell (3.0 mm \times 3.0 mm). The proposed pattern therefore increases the range of controllable capacitance to shift the cut-off frequency to its higher side.

Another advantage of the new cell pattern is its reduced field leakage characteristic. Suspended microstrip lines with the unit-cells detailed below were simulated. Far-field radiation patterns at different propagation frequencies are displayed in Fig. 7. It is seen that the cell design with small slots in the ground plane has a positive impact on radiation. For the conventional DGS cell, the apertures become an important source of radiation from the ground plane with increasing frequency, whereas the DMS unit-cell has smaller E-field patterns. For the L-slot DGS cell, the DMS behavior introduces a bandgap effect to regulate the current flowing around the periphery of the lattices. The diminished current flowing does not create any disruption in the responses of the microstrip line with L-slot DGS cell. At frequencies at which the inductive nature of the microstrip line is dominant [1], the radiation patterns of both DGS cells result to be similar (see Fig. 7a and 7b) showing a marginal improvement by the compact L-slot DGS, as expected.

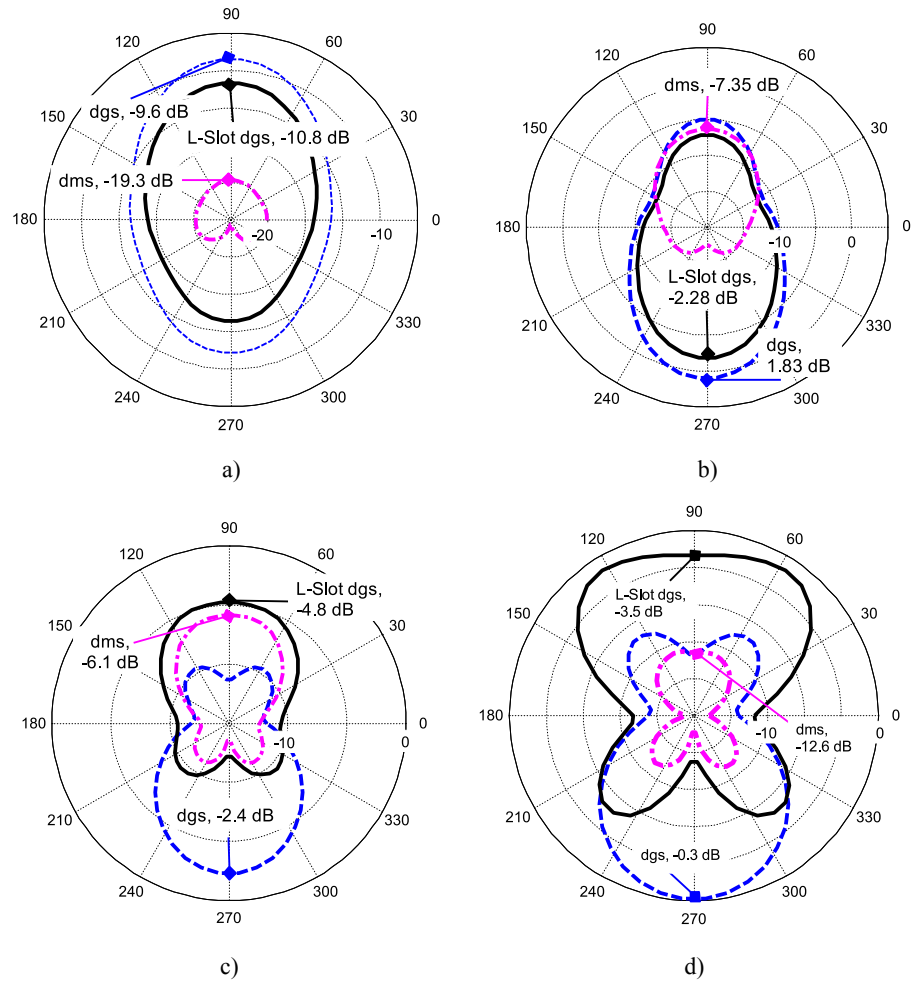


Fig. 7. Radiation pattern in *E*-plane of dumbbell-shaped DGS (dashed line), T-cell DMS (dash-dot line) and L-slot DGS (solid line) at a) 5.0 GHz, b) 7.7 GHz, c) 13.5 GHz and d) 15.0 GHz.

However, at 13.5 GHz, the DMS behavior minimizes the surface density current giving rise to a reduced magnetic flux flowing through the apertures. Notice that the DMS effect produces an E-field pattern similar to that of the DMS unit-cell (Fig. 7c). At 15 GHz (Fig. 7d), the relative improvement regarding the radiation underneath the ground plane is apparent.

5 Conclusions

We have presented a unit-cell based on DGS and DMS effects and its equivalent circuit-model. Frequency responses are modelled by a quarter-wave impedance transformer and a Butterworth-type resonant circuit. It is seen that DMS behavior results in a single attenuation pole with improved radiation effects and steep rejection bands in the frequency band of interest. We expect to apply the proposed cell pattern to create compact broadband periodic structures.